Nano Research

ISSN 1998-0124 CN 11-5974/O4
https://doi.org/10.1007/s12274-022-4751-2

Research Article

Fabricating ion-conducting channel in SU-8 matrix for high-performance patternable polymer electrolytes

Tianzhao Li[§], Xuelei Pan[§], Zhongzhuo Yang, Fang Liu, Kesong Yu, Lin Xu (✉), and Liqiang Mai (✉)

State Key Laboratory of Advanced Technology for Materials Synthesis and Processing, Wuhan University of Technology, Wuhan 430070, China
[§] *Tianzhao Li and Xuelei Pan contributed equally to this work.*

Received: 16 April 2022 / **Revised:** 29 June 2022 / **Accepted:** 8 July 2022

ABSTRACT

Advances in electrochemical energy storage technologies drive the need for battery safety performance and miniaturization, which calls for the easily processable polymer electrolytes suitable for on-chip microbattery technology. However, the low ionic conductivity of polymer electrolytes and poor-patternable capabilities hinder their application in microdevices. Herein, we modified SU-8, as the matrix material, by poly(ethylene oxide) (PEO) with lithium salts to obtain a patternable lithium-ion polymer electrolyte. Due to the highly amorphous state and more Li-ion transport pathways through blending effect and the increase in number of epoxides, the ionic conductivity of achieved sample is increased by an order of magnitude to 2.9×10^{-4} S·cm^{-1} in comparison with the SU-8 sample at 50 °C. The modified SU-8 exhibits good thermal stability (> 150 °C), mechanical properties (elastic modulus of 1.52 GPa), as well as an electrochemical window of 4.3 V. Half-cell and microdevice were fabricated and tested to verify the possibility of the micro-sized on-chip battery. All of these results demonstrate a promising strategy for the integration of on-chip batteries with microelectronics.

KEYWORDS

polymer electrolytes, patternable electrolytes, on-chip battery, lithium-ion battery

1 Introduction

With the advancement of electrochemical energy storage technology, lithium-ion batteries (LIBs) have been widely applied in electric vehicles and portable electronic devices [1–3]. However, the use of commercial LIBs has been greatly limited due to safety concerns of liquid electrolytes, such as flammability and Li dendrite penetration [4–6]. In comparison with liquid organic electrolytes, solid electrolytes possess the advantages of high mechanical strength, non-flammability, and high energy density, thereby becoming an important route to high-performance batteries [7, 8]. This is also the reason why solid-state electrolytes (SSEs) are deemed to be the most promising next-generation battery technology [9]. Among them, polymer electrolytes, as one of the most common SSEs, have attracted extensive attention due to their good compatibility with electrodes and ease of manufacture [10].

The revolution of solid-state batteries brings new opportunities to push large-scale batteries to a higher stage, especially for portable electronics and electrical vehicles. Meanwhile, with the continuous development of embedded hardware, microdevices such as microsensors, nano-robots, and micro-electromechanical systems (MEMS) continue to benefit from miniaturization and integration in the era of the Internet of Things (IoT) [11–13]. Owing to the slow progress in minimization of energy storage components, the power supply for these microdevices often becomes an important factor limiting the miniaturization of devices. Studies have shown that the miniaturization of electrochemical energy storage devices is far behind Moore's Law, with an average annual improvement of only approximately 10% [14, 15]. On-chip battery, also known as electrochemical energy storage at the point of load, is a progressive microelectronic technology that can effectively reduce I/O switching noise and energy loss [16, 17]. In recent years, some progress has been made in microfabrication for on-chip battery, such as nanoimprint and three-dimensional (3D) printing, but the low energy density limits the application of these devices [18–20]. How to obtain devices with higher energy density and fabricate electrodes as well as electrolytes with geometric control at the micrometer scale has become the key to carrying forward the integration of on-chip battery with microelectronics.

The current mature microfabrication techniques, such as photolithography and electron beam lithography have been widely used in the fabrication of electrochemical energy storage microdevices [21–24]. These developed processes are compatible with conventional semiconductor processes and can construct patterns with high spatial resolution. But the major problem with direct lithography is the lack of photolithographic SSEs with high resolution patterns, excellent mechanical properties, and high ionic conductivity. Recent research about SSEs mainly focused on ultraviolet (UV)-cured polymers. Dunn's group modified a well-known photoresist SU-8 by $LiClO_4$ exhibiting an ionic conductivity of 5.2×10^{-5} S·cm^{-1} with a wide electrochemical window (> 5 V) [25]. Although photopatternable SSEs are obtained by this method, the low ionic conductivity limits the prospects of electrolytes application. Hence, a patternable high-performance polymer electrolyte is urgently needed to be

Address correspondence to Lin Xu, linxu@whut.edu.cn; Liqiang Mai, mlq518@whut.edu.cn

developed to realize continuous and positioned fabrication of the on-chip energy device.

In this work, we used SU-8, an epoxy-based negative photoresist, as the matrix material and added poly(ethylene oxide) (PEO) with bis(trifluoromethane)sulfonimide lithium salt (LiTFSI) as the modifying agents to modify SU-8 (indicated by the acronym PSU-8). A photopatternable lithium-ion polymer electrolyte with circular features 50 μm in diameter was developed. Compared with SU-8 lack of PEO, the ionic conductivity of PSU-8 is improved by an order of magnitude, reaching 2.9×10^{-4} S·cm^{-1} at 50 °C. Meanwhile, PSU-8 exhibits an electrochemical window of 4.3 V and excellent mechanical and thermal properties. Furthermore, to verify the possibility of on-chip battery, Au|polymer electrolytes|Au microdevice prototypes were built and tested directly on silicon wafers, showing the prospect of using PSU-8 for microdevices.

2 Experimental

2.1 Preparation of PSU-8 sample

0.5 g PEO and 0.32g LiTFSI were dissolved in 8 mL anhydrous acetonitrile (ACN), and then stirred at 60 °C for 6 h. After the PEO has been evenly dispersed, 1.16 g SU-8 was incorporated into the above solution rapidly and agitated for 1 h. When preparing thin films for electrochemical measurement, spin-coating was performed on stainless steel (SS) sheets (Φ16.2 mm × 0.5 mm) at 500 rpm for 10 s and 4,000 rpm for 40 s using a spin coater. The sample was then baked under vacuum at 60 °C for 12 h to remove the solvent before patterning. The PSU-8 sample was exposed to the UV wavelength of 365 nm by an ABM contact mask aligner (model: ABM/6/350/NUV/DCCD/BSV/M), and exposure baked at 70 °C for 1 h to polymerize samples. Subsequently, PSU-8 was developed in propylene glycol monomethyl ether acetate (PGMEA) and diluted acetonitrile for 5 min and 30 s, respectively. After development, PSU-8 sample was quickly transferred to an argon-filled glove box to prevent long-term exposure to environmental conditions. The thickness of PSU-8 was 12 μm measured by micrometer caliper. During the preparation process, the PSU-8 sample was directly prepared on the electrode surface, which largely avoided the break of the sample and ensured its integrity. SU-8 sample containing the same mass fraction of lithium salts was prepared and tested by the above steps.

2.2 Materials characterization

X-ray diffraction (XRD) patterns were obtained using a Bruker D8 discover X-ray diffractometer with Cu Kα radiation. The, morphology information of SU-8 and PSU-8 were collected by a field-emission scanning electron microscopy (FESEM, JEOL-7100F) after gold spraying. Energy dispersive spectrometer (EDS) mapping was measured by an Oxford IE250 system. The Fourier transform infrared (FT-IR, NICOLET-6700) spectroscopy (400–4,000 cm^{-1}) was performed at room temperature. The Raman spectra were acquired by Horiba LabRAM HR Evolution using a 532 nm excitation laser. The thermal stability was measured by thermogravimetric analysis (TGA) using a NETZSCH STA 449F5 instrument in the temperature range of 25–800 °C in the presence of argon gas at the heating rate of 10 °C·min^{-1}. To determine the mechanical behavior of SU-8 and PSU-8, the elastic modulus and hardness were measured using nanoindentation (TI-980, Bruker-Hysitron). The thickness of SU-8 and PSU-8 was measured using a micrometer caliper (Shanghai measuring tool factory, China).

2.3 Electrochemical measurements

Electrochemical impedance spectroscopy (EIS) was tested by a blocking SS|polymer electrolytes|SS cell using Autolab PGSTAT302N with an amplitude of 10 mV from 1 Hz to 1 MHz. The electrochemical stability window was tested by linear sweep voltammetry on a lithium|SSE|SS cell from open-circuit voltage to 6.5 V at a scan rate of 5 mV·s^{-1}. CR2016 coin cells were assembled with amorphous silicon (a-Si) electrode, polymer electrolytes, and commercial lithium metal anodes via ordinal stacking. The galvanostatic charge–discharge performance of a-Si|PSU-8|Li half-cells was measured via a multichannel battery testing system (LAND CT2001A). The $LiFePO_4$|PSU-8|Li battery was assembled and tested in the same way as the half cell. During battery assembly, 5 μL electrolyte (1.0 M $LiPF_6$ in EC:DMC:EMC = 1:1:1 vol.%) was added to the surface of samples and placed for 3 h. In order to simulate the working environment of the on-chip battery, the electrochemical measurements were carried out at 50 °C.

3 Results and discussion

To accommodate the process requirements of on-chip devices, we first attempted to develop a patternable polymer electrolyte fabrication pathway. This work adopts SU-8 as the matrix material and PEO with high ionic conductivity as the modifying agent. As a usual solid polymer electrolyte, PEO-based electrolytes rely on (–EO–) oligoether segments for fast ion conduction, possesses a strong ability to dissolve lithium ions, and can accomplish well blending with SU-8 taking epoxy groups at the end [26]. Figure 1 shows the schematic representation of the preparation steps for PSU-8 patterns by the UV lithography. SU-8 photoresist, PEO, and LiTFSI were dissolved in ACN and subsequently spin-coated onto substrates. Then the acetonitrile was evaporated to form the films. The obtained film was patterned using photomask and UV lithography. For polymerizing PSU-8 samples, the specimens were then exposure baked at 70 °C for 1 h. At last, PSU-8 samples were developed in SU-8 developer to obtain patterns.

Scanning electron microscopy (SEM) images of PSU-8 and SU-8 are shown in Figs. S1 and S2 in the Electronic Supplementary Material (ESM), respectively. Compared with PSU-8 sample, SU-8 is free of wrinkles and possesses a smoother surface owing to no solvent evaporation during the preparation. Furthermore, SEM

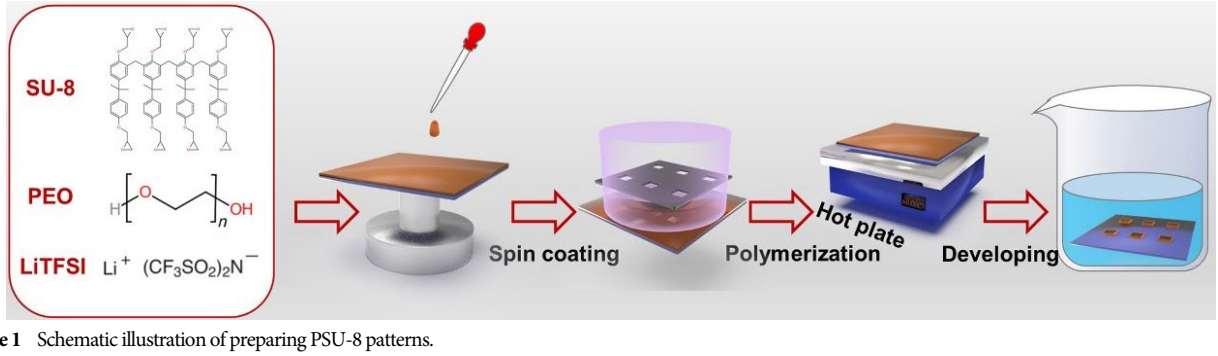

Figure 1 Schematic illustration of preparing PSU-8 patterns.

images of two samples show the polymer electrolyte has fine homogeneity and miscibility. The uniform distribution of the various components in PSU-8 and SU-8 is further confirmed by EDS observed microcracks of the surface, which are formed by scratching the sample's surface with sharp tweezers. Besides, these signals of fluorine and sulfur are attributed only to salts.

XRD patterns of PEO, SU-8, and PSU-8 are displayed in Fig. 2(a). As shown in the spectrum of PEO, there are two sharp diffraction peaks at 2θ = 19.2° and 23.4°, demonstrating a high crystallinity of the pure PEO. However, the PSU-8 spectrum shows only a broad signal and the absence of clear diffraction peaks, suggesting the highly amorphous state of the sample and proving the benefit of the blending. The blending of SU-8 and PEO to obtain PSU-8 can be further proved by the Raman spectra (Fig. S3 in the ESM). In addition, after the UV irradiation and postexposure baking, the crosslinking network with disordered architecture was formed due to the UV-derived polymerization; hence, the reaction may reduce the crystallization of PEO chains [27]. Meanwhile, owing to the fact that the solvated ions in the polymer chain lengthen the physical distance between reactive epoxide groups and raise the energy required for polymerization, the degree of crosslinking may be also decreased. For PEO-based polymer electrolytes, since the adsorption and transport of lithium ions mainly occur in the amorphous regions, the lower crystallinity can promote the transport of lithium ions between PEO chains, thereby improving electrolytes ionic conductivity [28].

During UV irradiation, the eight epoxy groups in the SU-8 monomer are opened by the photoinitiator contained in the photoresist. Under the high temperature of postexposure baking, the crosslinking reaction occurs between these adjacent groups to form ether linkages (Fig. 2(b)). The reaction process can be characterized by FTIR spectroscopy. The changes in the absorption peaks of the samples before and after the reaction are shown in Figs. 2(c)–2(e), respectively. The three characteristic absorption peaks are attributed to the variations of hydroxyl (3,430 cm^{-1}), ether (1,100 cm^{-1}), and epoxide (907 cm^{-1}). In contrast with non-crosslinked SU-8, the peaks of hydroxyl group as well as epoxide group increase, and the other group decreases for the samples fully crosslinked.

The high ionic conductivity of polymer electrolytes in lithium-ion batteries is the basis for achieving good battery performance. The PSU-8 and SU-8 were assembled into batteries through SS|polymer electrolytes|SS symmetric cells (Fig. S4 in the ESM) to measure the EIS. The impedance spectroscopy of PSU-8 was tested at the temperature from 20 to 70 °C in frequency from 1 Hz to 1 MHz (Fig. 3(a)). It can be seen that the PSU-8 shows a low ionic resistance of 2.0 Ω at 50 °C. Moreover, the corresponding ionic conductivity of PSU-8 at the different temperatures can be calculated by the formula, and the ionic conductivity of PSU-8 is 2.9×10^{-4} S·cm^{-1} at 50 °C. Meanwhile, the ionic conductivity of SU-8 at 50 °C was also obtained, which is 3.3×10^{-5} S·cm^{-1}. Due to the blending effect produced by the addition of PEO and the excellent lithium ions transport properties for PEO, the ionic conductivity of polymer electrolytes has been greatly improved [29]. Through further computation, the Arrhenius curve of PSU-8 can be obtained by fitting, as shown in Fig. 3(b). The activation energy (E_a) of Li-ions transport for PSU-8 is computed to be 0.11 eV. The value is higher than the activation energy of liquid electrolytes (≈ 0.1 eV) and lower than that of previously reported SU-8 gel polymer electrolytes (≈ 0.16 eV) [25]. Since PEO has Lewis basic centers, the epoxide groups in PEO can be complexed with lithium ions to transport Li-ions. The added PEO increases the number of epoxides in the matrix, thereby improving the ionic conductivity of the polymer electrolytes [30, 31].

The electrochemical stability windows (ESW) of polymer electrolytes were characterized via linear sweep voltammetry (LSV) using Li|polymer electrolytes|SS cells. Figure 3(c) shows the oxidation potential of PSU-8 and SU-8 is 4.3 and 5.0 V, respectively. The result suggests that although the addition of PEO makes the oxidation potential of PSU-8 polymer electrolytes drop, it still maintains a higher potential than pure poly(ethylene glycol) (PEG) [32]. Consequently, the electrochemical stability of the PSU-8 polymer electrolyte makes it possible to use PSU-8 with a high-voltage cathode material, such as $LiFeO_4$ operating at about 3.5 V and layered metal oxides [33].

It is well known that polymer electrolytes must have sufficiently excellent mechanical properties to prevent short circuits caused by lithium dendrites. In Fig. 3(d), the mechanical performance of samples without liquid electrolytes was tested by nanoindentation

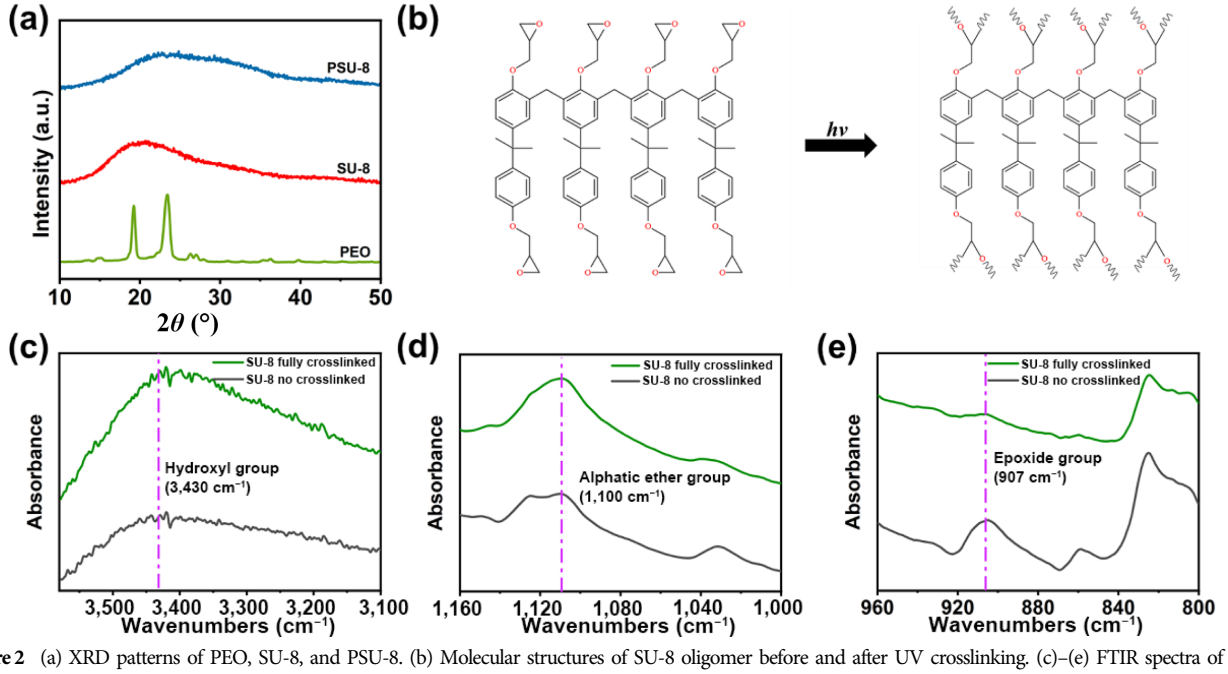

Figure 2 (a) XRD patterns of PEO, SU-8, and PSU-8. (b) Molecular structures of SU-8 oligomer before and after UV crosslinking. (c)–(e) FTIR spectra of SU-8 before and after crosslinking reaction.

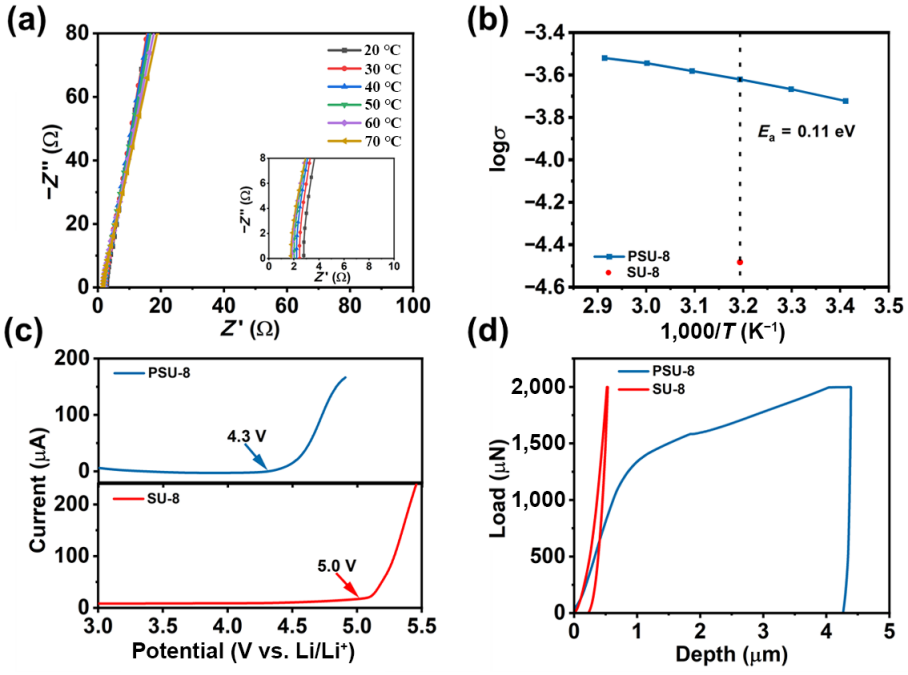

Figure 3 (a) EIS of PSU-8 within frequency from 1 Hz to 1 MHz at various temperature, inset: magnified high frequency region. (b) Arrhenius plots of PSU-8 and SU-8. (c) Electrochemical stability windows of PSU-8 and SU-8. (d) Load vs. depth curve for PSU-8 and SU-8 measured by nanoindentation.

measurements. The characterization results indicate that the elastic modulus and hardness of SU-8 are 4.64 and 0.29 GPa, respectively. In comparison with SU-8, the elastic modulus and hardness of PSU-8 decrease to a certain extent, which are 1.52 GPa and 2.68 MPa, respectively, due to the addition of PEO. Generally speaking, the elastic modulus of polymer electrolytes is less than the minimum value (≈ 8.5 GPa) to suppress the growth of lithium dendrites, thus greatly limiting the application of electrolytes in lithium-ion batteries [34–36]. Previous studies have shown that the elastic modulus of crosslinked PEO with LiTFSI is merely 0.033 GPa, which is much lower than the experimental specimens (Table S1 in the ESM) [37]. Therefore, compared with other polymer electrolytes, PSU-8 possessing excellent mechanical properties can do better in preventing Li dendrites.

The thermal stability of polymer electrolytes can be demonstrated by TGA in Fig. 4(a). As shown by the curve, the pure SU-8 without lithium salts is thermally stable up to 300 °C. For the blending PSU-8, due to the mixed lithium salts and PEO, the crosslinking degree of SU-8 decreases, thereby reducing the thermal stability, reaching 150 °C. Nevertheless, PSU-8 still reaches a high stable temperature, as consistent with previous studies [38–40]. In summary, the assembly of PSU-8 into the lithium-ion batteries can ensure a desirable safety performance.

To further explore the electrochemical performance of PSU-8, a-Si|PSU-8|Li half-cells were assembled and tested (Fig. 4(b)). Amorphous silicon was deposited onto the surface of the copper foil by direct-current (DC) magnetron sputtering. Figure 4(c) illustrates an obvious broad signal, but no characteristic diffraction peaks of crystalline silicon appear, indicating that the silicon film obtained by magnetron sputtering is amorphous. Apart from XRD pattern, Raman spectra also prove the point. In Fig. S5(b) in the ESM, comparing silicon film with silicon wafer, it is found that the characteristic peak of amorphous silicon is red-shifted relative to the standard peak of single-crystal silicon, from 525 to 482 cm^{-1} [41, 42]. From the SEM images, it can be seen that the thickness of amorphous silicon is 1.44 μm (Fig. S5(a) in the ESM) and it presents dense surface morphology (Fig. 4(c)). The galvanostatic charge–discharge curves of a-Si/Li half-cells with polymer electrolytes PSU-8 operating at the current density of 1 A/g with voltage range of 0.01–1.50 V at 50 °C are displayed in Fig. 4(d). The smoothly sloping voltage plateau in the charge–discharge curves corresponds to the potential during insertion/extraction of lithium ions in a-Si. The irreversible capacity in the first discharge is attributed to the formation of solid electrolyte interphase (SEI). During cycling, the capacity fading of the batteries is due to the volume change and stress strain of amorphous silicon at time of insertion/extraction of lithium ions, resulting in the structural collapse and pulverization of amorphous silicon [43, 44]. A Celgard membrane was chosen as the control sample, and the results are shown in Fig. 4(e). The profiles reflect the charge–discharge curves of batteries in the second cycle. It can be seen that the specific capacity of PSU-8 is significantly higher than that of the control sample at 50 °C. Additionally, the half-cells after different cycles were tested EIS (Fig. 4(f)). The Nyquist plots indicate that the impedance of half-cells increases after the second cycle and remains stable after the 20th cycle, which could be ascribed to the formation of SEI. In the meantime, the fit curves of impedance spectroscopy and fitted values are presented in Figs. S6 and S7 in the ESM. To confirm the function of the PEO modified SU-8 electrolyte, the $LiFePO_4$|PSU-8|Li battery was assembled and tested. During the voltage range of 2.8–4.0 V at 0.3 C, the LFP full cells display a stable long-term cycle performance (Fig. S8 in the ESM). The PSU-8 sample has higher capacity retention (136.8 $mAh{\cdot}g^{-1}$ and 93.0% retention) and high Coulombic efficiency (more than 91.0%).

Fabrication of polymer electrolytes with geometric control at the micrometer scale enables the integration of on-chip battery with microelectronics using conventional semiconductor processes. To characterize the performance of specimens in microdevices, Au|polymer electrolytes|Au symmetric cells were assembled (Fig. 5(a)). The Au electrodes were fabricated by thermal evaporation deposition onto the Si wafer (Fig. S9(a) in the ESM). Afterwards, the polymer electrolytes were designed as a rectangle on Au electrodes by UV lithography (Fig. S9(b) in the ESM). In Fig. 5(b), the Nyquist plots are applied to further investigate electrochemical characteristics of PSU-8 and SU-8. The impedance of PSU-8 is significantly smaller than that of SU-8, which proves the great potential of this electrolyte for on-chip

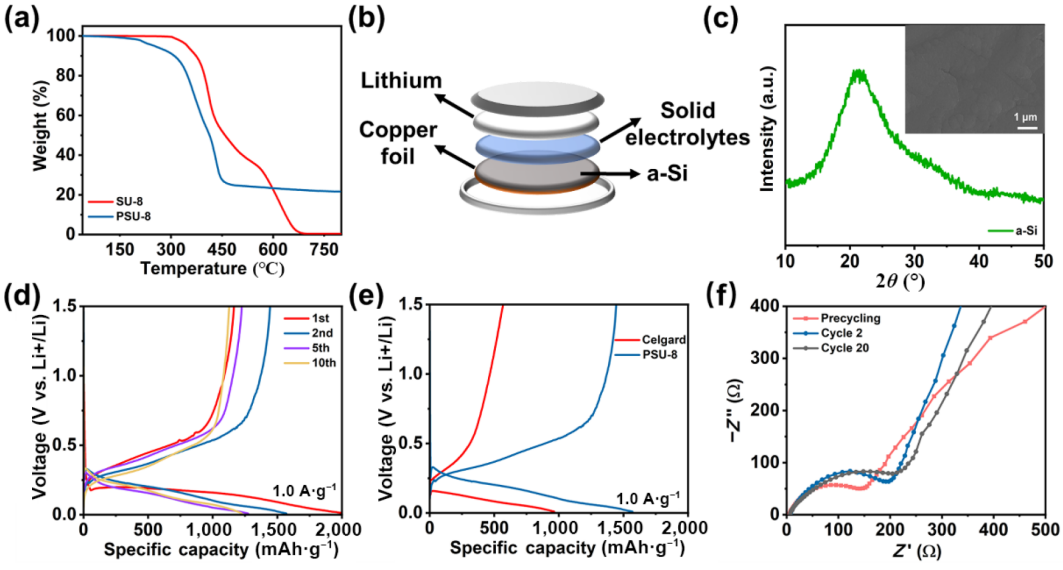

Figure 4 (a) TGA profiles of PSU-8 and SU-8. (b) Schematic illustration of a-Si|PSU-8|Li half-cells. (c) XRD patterns of a-Si, inset: SEM image of a-Si. (d) The galvanostatic charge–discharge curves of a-Si|PSU-8|Li half-cells at 1.0 A/g. (e) The second galvanostatic cycle of a-Si/PSU-8/Li and a-Si/Celgard/Li half-cells at 1.0 A·g^{-1}; note: the data here are extracted from Fig. 4(d). (f) Nyquist plot for a-Si/PSU-8/Li half-cells comparing before cycling, after the second cycle, and after the 20th cycle.

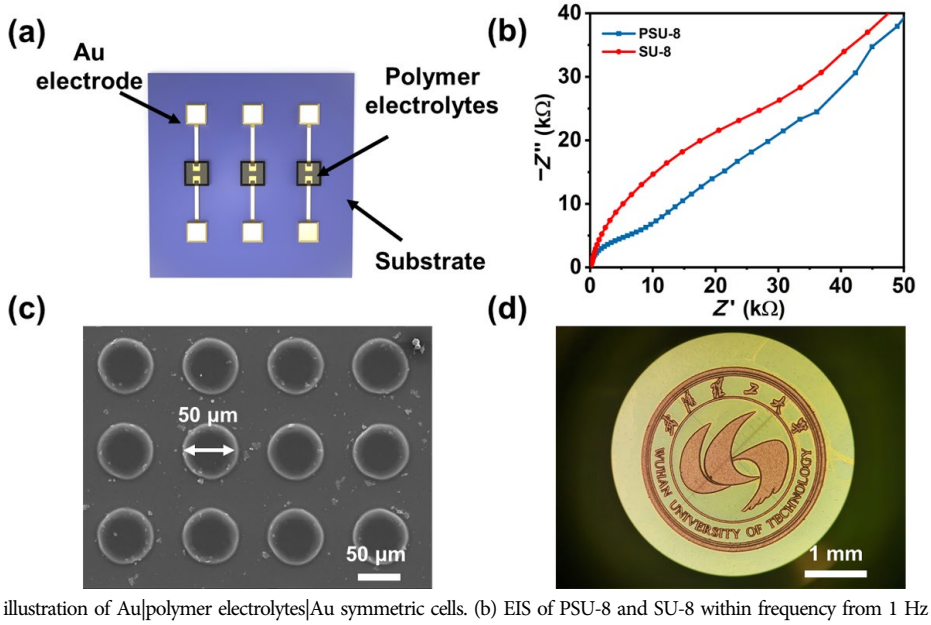

Figure 5 (a) Schematic illustration of Au|polymer electrolytes|Au symmetric cells. (b) EIS of PSU-8 and SU-8 within frequency from 1 Hz to 1 MHz at 50 °C. (c) SEM image of PSU-8 with features: circular, 50 μm in diameter. (d) Optical image of the PSU-8 electrolyte in the shape of the school badge.

energy storage devices. PSU-8 samples were further patterned on the silicon wafer by the masks with circular or square features. To demonstrate the patternable properties of the samples, photomasks of different diameters were designed and used to pattern the samples. Figure 5(c) illustrates that PSU-8 has a 50 μm scale size, and the result indicates that PSU-8 can be directly patterned on-chip with a high spatial resolution. Furthermore, other optical photos and SEM images are shown in Fig. 5(d) and Fig. S10 in the ESM, which all demonstrate a good patterning property. The discovery is important, as it heralds the possibility of PSU-8 designing battery arrays with tailored voltages and currents for given applications via connecting individual cells of specific chemistry in series and parallel, respectively.

4 Conclusions

In summary, a patternable SU-8 based polymer electrolyte was successfully prepared via modifying agents PEO with LiTFSI. In contrast to SU-8, the ionic conductivity of PSU-8 samples is improved by an order of magnitude and enhanced to 2.9 × 10^{-4} S·cm^{-1}, which is owing to more Li-ion transport pathways through blending effect and the increase in number of epoxides. Apart from this, PSU-8 exhibits an electrochemical window of 4.3 V, good thermal stability (> 150 °C), as well as excellent mechanical properties (elastic modulus of 1.52 GPa, which is about 50 times that of PEO). The half-cell was assembled on the a-Si obtained by magnetron sputtering, and the PSU-8 displayed higher specific capacity in contrast with the Celgard separator. Finally, a microdevice, Au|polymer electrolytes|Au symmetric cell, was fabricated and tested for electrochemical impedance spectroscopy. Due to its good electrochemical, mechanical and thermal properties, PSU-8 can be used to fabricate stand-alone MEMS components, and at the same time, it may also be used as an electrolyte for preparation of on-chip battery.

Acknowledgements

This work was supported by the National Key Research and

Development Program of China (No. 2020YFA0715000), the National Natural Science Foundation of China (Nos. 51802239, 51832004), Foshan Xianhu Laboratory of the Advanced Energy Science and Technology Guangdong Laboratory (Nos. XHT2020-005, XHT2020-003), and the Innovation and Entrepreneurship Training Program of School of Materials Science and Engineering, Wuhan University of Technology (No. CY202031).

Electronic Supplementary Material: Supplementary material (SEM and EDS of PSU-8 and SU-8 (Figs. S1 and S2 in the ESM), Raman spectra of PEO, SU-8, and PSU-8 (Fig. S3 in the ESM), schematic illustration of SS|PSU-8|SS half-cells (Fig. S4 in the ESM), SEM and Raman spectra of a-Si (Fig. S5 in the ESM), fit curve and fitted values of a-Si|PSU-8|Li half-cells (Figs. S6 and S7 in the ESM), cycle performance of the LiFePO4|PSU-8|Li battery (Fig. S8 in the ESM), optical image and SEM image of PSU-8 (Figs. S9 and S10 in the ESM), and comparisons of this work and previous reports (Table S1 in the ESM) in different polymer electrolytes) is available in the online version of this article at https://doi.org/10.1007/s12274-022-4751-2.

References

[1] Armand, M.; Tarascon, J. M. Building better batteries. *Nature* **2008**, *451*, 652–657.

[2] Lin, D. C.; Liu, Y. Y.; Cui, Y. Reviving the lithium metal anode for high-energy batteries. *Nat. Nanotechnol.* **2017**, *12*, 194–206.

[3] Yu, K. S.; Pan, X. L.; Zhang, G. B.; Liao, X. B.; Zhou, X. B.; Yan, M. Y.; Xu, L.; Mai, L. Q. Nanowires in energy storage devices: Structures, synthesis, and applications. *Adv. Energy Mater.* **2018**, *8*, 1802369.

[4] Lin, X. D.; Yu, J.; Effat, M. B.; Zhou, G. D.; Robson, M. J.; Kwok, S. C. T.; Li, H. J.; Zhan, S. Y.; Shang, Y. L.; Ciucci, F. Ultrathin and non-flammable dual-salt polymer electrolyte for high-energy-density lithium-metal battery. *Adv. Funct. Mater.* **2021**, *31*, 2010261.

[5] Xu, L.; Tang, S.; Cheng, Y.; Wang, K. Y.; Liang, J. Y.; Liu, C.; Cao, Y. C.; Wei, F.; Mai, L. Q. Interfaces in solid-state lithium batteries. *Joule* **2018**, *2*, 1991–2015.

[6] Fan, L.; Wei, S. Y.; Li, S. Y.; Li, Q.; Lu, Y. Y. Recent progress of the solid-state electrolytes for high-energy metal-based batteries. *Adv. Energy Mater.* **2018**, *8*, 1702657.

[7] Thangadurai, V.; Narayanan, S.; Pinzaru, D. Garnet-type solid-state fast Li ion conductors for Li batteries: Critical review. *Chem. Soc. Rev.* **2014**, *43*, 4714–4727.

[8] Zheng, H. P.; Wu, S. P.; Tian, R.; Xu, Z. M.; Zhu, H.; Duan, H. N.; Liu, H. Z. Intrinsic lithiophilicity of Li-garnet electrolytes enabling high-rate lithium cycling. *Adv. Funct. Mater.* **2020**, *30*, 1906189.

[9] Xia, Y. Y.; Xu, N.; Du, L. L.; Cheng, Y.; Lei, S. L.; Li, S. J.; Liao, X. B.; Shi, W. C.; Xu, L.; Mai, L. Q. Rational design of ion transport paths at the interface of metal-organic framework modified solid electrolyte. *ACS Appl. Mater. Interfaces* **2020**, *12*, 22930–22938.

[10] Dong, D. R.; Zhou, B.; Sun, Y. F.; Zhang, H.; Zhong, G. M.; Dong, Q. Y.; Fu, F.; Qian, H.; Lin, Z. Y.; Lu, D. R. et al. Polymer electrolyte glue: A universal interfacial modification strategy for all-solid-state Li batteries. *Nano Lett.* **2019**, *19*, 2343–2349.

[11] Xia, S. L.; Ni, J. F.; Savilov, S. V.; Li, L. Oxygen-deficient Ta_2O_5 nanoporous films as self-supported electrodes for lithium microbatteries. *Nano Energy* **2018**, *45*, 407–412.

[12] Pan, X. L.; Hong, X. F.; Xu, L.; Li, Y. X.; Yan, M. Y.; Mai, L. Q. On-chip micro/nano devices for energy conversion and storage. *Nano Today* **2019**, *28*, 100764.

[13] Fan, X. Y.; Liu, X. R.; Hu, W. B.; Zhong, C.; Lu, J. Advances in the development of power supplies for the internet of everything. *InfoMat* **2019**, *1*, 130–139.

[14] Rolison, D. R.; Nazar, L. F. Electrochemical energy storage to power the 21st century. *MRS Bull.* **2011**, *36*, 486–493.

[15] Choi, C.; Robert, K.; Whang, G.; Roussel, P.; Lethien, C.; Dunn, B. Photopatternable hydroxide ion electrolyte for solid-state micro-supercapacitors. *Joule* **2021**, *5*, 2466–2478.

[16] El-Kady, M. F.; Kaner, R. B. Scalable fabrication of high-power graphene micro-supercapacitors for flexible and on-chip energy storage. *Nat. Commun.* **2013**, *4*, 1475.

[17] Wu, Z. S.; Feng, X. L.; Cheng, H. M. Recent advances in graphene-based planar micro-supercapacitors for on-chip energy storage. *Natl. Sci. Rev.* **2014**, *1*, 277–292.

[18] Zhang, F.; Wei, M.; Viswanathan, V. V.; Swart, B.; Shao, Y. Y.; Wu, G.; Zhou, C. 3D printing technologies for electrochemical energy storage. *Nano Energy* **2017**, *40*, 418–431.

[19] Zhu, C.; Liu, T. Y.; Qian, F.; Chen, W.; Chandrasekaran, S.; Yao, B.; Song, Y.; Duoss, E. B.; Kuntz, J. D.; Spadaccini, C. M. et al. 3D printed functional nanomaterials for electrochemical energy storage. *Nano Today* **2017**, *15*, 107–120.

[20] Kim, S. H.; Choi, K. H.; Cho, S. J.; Choi, S.; Park, S.; Lee, S. Y. Printable solid-state lithium-ion batteries: A new route toward shape-conformable power sources with aesthetic versatility for flexible electronics. *Nano Lett.* **2015**, *15*, 5168–5177.

[21] Mai, L. Q.; Dong, Y. J.; Xu, L.; Han, C. H. Single nanowire electrochemical devices. *Nano Lett.* **2010**, *10*, 4273–4278.

[22] Mai, L. Q.; Tian, X. C.; Xu, X.; Chang, L.; Xu, L. Nanowire electrodes for electrochemical energy storage devices. *Chem. Rev.* **2014**, *114*, 11828–11862.

[23] Xu, X.; Yan, M. Y.; Tian, X. C.; Yang, C. C.; Shi, M. Z.; Wei, Q. L.; Xu, L.; Mai, L. Q. *In situ* investigation of Li and Na ion transport with single nanowire electrochemical devices. *Nano Lett.* **2015**, *15*, 3879–3884.

[24] Zhang, P. P.; Zhu, F.; Wang, F. X.; Wang, J. H.; Dong, R. H.; Zhuang, X. D.; Schmidt, O. G.; Feng, X. L. Stimulus-responsive micro-supercapacitors with ultrahigh energy density and reversible electrochromic window. *Adv. Mater.* **2017**, *29*, 1604491.

[25] Choi, C. S.; Lau, J.; Hur, J.; Smith, L.; Wang, C. L.; Dunn, B. Synthesis and properties of a photopatternable lithium-ion conducting solid electrolyte. *Adv. Mater.* **2018**, *30*, 1703772.

[26] Xue, Z. G.; He, D.; Xie, X. L. Poly (ethylene oxide)-based electrolytes for lithium-ion batteries. *J. Mater. Chem. A* **2015**, *3*, 19218–19253.

[27] Zhang, Y. H.; Lu, W.; Cong, L. N.; Liu, J.; Sun, L. Q.; Mauger, A.; Julien, C. M.; Xie, H. M.; Liu, J. Cross-linking network based on poly (ethylene oxide): Solid polymer electrolyte for room temperature lithium battery. *J. Power Sources* **2019**, *420*, 63–72.

[28] Das, D.; Chandrasekaran, A.; Venkatram, S.; Ramprasad, R. Effect of crystallinity on Li adsorption in polyethylene oxide. *Chem. Mater.* **2018**, *30*, 8804–8810.

[29] Wong, D. H. C.; Vitale, A.; Devaux, D.; Taylor, A.; Pandya, A. A.; Hallinan, D. T.; Thelen, J. L.; Mecham, S. J.; Lux, S. F.; Lapides, A. M. et al. Phase behavior and electrochemical characterization of blends of perfluoropolyether, poly (ethylene glycol), and a lithium salt. *Chem. Mater.* **2015**, *27*, 597–603.

[30] Rajendran, S.; Mahendran, O.; Kannan, R. Characterisation of [(1−*x*) PMMA–*x*PVDF] polymer blend electrolyte with Li^+ ion. *Fuel* **2002**, *81*, 1077–1081.

[31] Reddy, M. J.; Chu, P. P.; Kumar, J. S.; Rao, U. V. S. Inhibited crystallization and its effect on conductivity in a nano-sized fe oxide composite peo solid electrolyte. *J. Power Sources* **2006**, *161*, 535–540.

[32] Yang, X. F.; Jiang, M.; Gao, X. J.; Bao, D. N.; Sun, Q.; Holmes, N.; Duan, H.; Mukherjee, S.; Adair, K.; Zhao, C. T. et al. Determining the limiting factor of the electrochemical stability window for PEO-based solid polymer electrolytes: Main chain or terminal-OH group? *Energy Environ. Sci.* **2020**, *13*, 1318–1325.

[33] Appetecchi, G. B.; Hassoun, J.; Scrosati, B.; Croce, F.; Cassel, F.; Salomon, M. Hot-pressed, solvent-free, nanocomposite, PEO-based electrolyte membranes: II. *All solid-state Li/LiFePO$_4$ polymer batteries. J. Power Sources* **2003**, *124*, 246–253.

[34] Yu, S.; Schmidt, R. D.; Garcia-Mendez, R.; Herbert, E.; Dudney, N. J.; Wolfenstine, J. B.; Sakamoto, J.; Siegel, D. J. Elastic properties of the solid electrolyte $Li_7La_3Zr_2O_{12}$ (LLZO). *Chem. Mater.* **2016**, *28*, 197–206.

[35] Zhang, J. J.; Zhao, J. H.; Yue, L. P.; Wang, Q. F.; Chai, J. C.; Liu, Z. H.; Zhou, X. H.; Li, H.; Guo, Y. G.; Cui, G. L. et al. Safety-

reinforced poly (propylene carbonate)-based all-solid-state polymer electrolyte for ambient-temperature solid polymer lithium batteries. *Adv. Energy Mater.* **2015**, *5*, 1501082.

[36] Fu, C. Y.; Venturi, V.; Kim, J.; Ahmad, Z.; Ells, A. W.; Viswanathan, V.; Helms, B. A. Universal chemomechanical design rules for solid-ion conductors to prevent dendrite formation in lithium metal batteries. *Nat. Mater.* **2020**, *19*, 758–766.

[37] Lin, D. C.; Yuen, P. Y.; Liu, Y. Y.; Liu, W.; Liu, N.; Dauskardt, R. H.; Cui, Y. A silica-aerogel-reinforced composite polymer electrolyte with high ionic conductivity and high modulus. *Adv. Mater.* **2018**, *30*, 1802661.

[38] Liang, W. F.; Shao, Y. F.; Chen, Y. M.; Zhu, Y. A 4 V cathode compatible, superionic conductive solid polymer electrolyte for solid lithium metal batteries with long cycle life. *ACS Appl. Energy Mater.* **2018**, *1*, 6064–6071.

[39] Wang, C.; Wang, T.; Wang, L. L.; Hu, Z. L.; Cui, Z. L.; Li, J. D.; Dong, S. M.; Zhou, X. H.; Cui, G. L. Differentiated lithium salt design for multilayered PEO electrolyte enables a high-voltage solid-state lithium metal battery. *Adv. Sci.* **2019**, *6*, 1901036.

[40] Liu, Y. L.; Zhao, Y.; Lu, W.; Sun, L. Q.; Lin, L.; Zheng, M.; Sun, X. L.; Xie, H. M. PEO based polymer in plastic crystal electrolytes for room temperature high-voltage lithium metal batteries. *Nano Energy* **2021**, *88*, 106205.

[41] Pollak, E.; Salitra, G.; Baranchugov, V.; Aurbach, D. In situ conductivity, impedance spectroscopy, and ex situ Raman spectra of amorphous silicon during the insertion/extraction of lithium. J. Phys. *Chem. C* **2007**, *111*, 11437–11444.

[42] Ma, T. Y.; Xu, H. Y.; Yu, X. N.; Li, H. Y.; Zhang, W. G.; Cheng, X. L.; Zhu, W. T.; Qiu, X. P. Lithiation behavior of coaxial hollow nanocables of carbon-silicon composite. *ACS Nano* **2019**, *13*, 2274–2280.

[43] Son, Y.; Sung, J.; Son, Y.; Cho, J. Recent progress of analysis techniques for silicon-based anode of lithium-ion batteries. *Curr. Opin. Electrochem.* **2017**, *6*, 77–83.

[44] Li, J. Y.; Li, G.; Zhang, J.; Yin, Y. X.; Yue, F. S.; Xu, Q.; Guo, Y. G. Rational design of robust Si/C microspheres for high-tap-density anode materials. *ACS Appl. Mater. Interfaces* **2019**, *11*, 4057–4064.